1.1 CHANTI

1.1.1 CHANTI Detector Requirements

The Charged ANTI (CHANTI) detector is required in order to reduce critical background induced by inelastic interactions of the beam with the collimator and the Gigatracker (GTK) stations as well as to tag beam halo muons in the region immediately close to the beam. The most critical events are the ones in which the inelastic interaction takes place in the last GTK station (GTK-3). In such cases, pions or other particles produced in the interaction, if emitted at low angle, can reach the straw tracker and mimic a K decay in the fiducial region. If no other track is detected, these events can appear like a signal event, i.e. one single π^+ in the final state. A GEANT4 simulation has shown that kaon inelastic interactions with GTK-3 happens in about $1/10^3$ cases, so that the combined rejection factors of the analysis cuts and the CHANTI veto must lead to a remaining inefficiency of 10^{-8}.

The purpose of the CHANTI is to identify inelastic interactions in the GTK by tagging particles at higher angles w.r.t. to the beam. This can be achieved by placing a number of guard counters right immediately after GTK3. At the same time the CHANTI can also veto beam halo (muons) in the region closest to the beam.

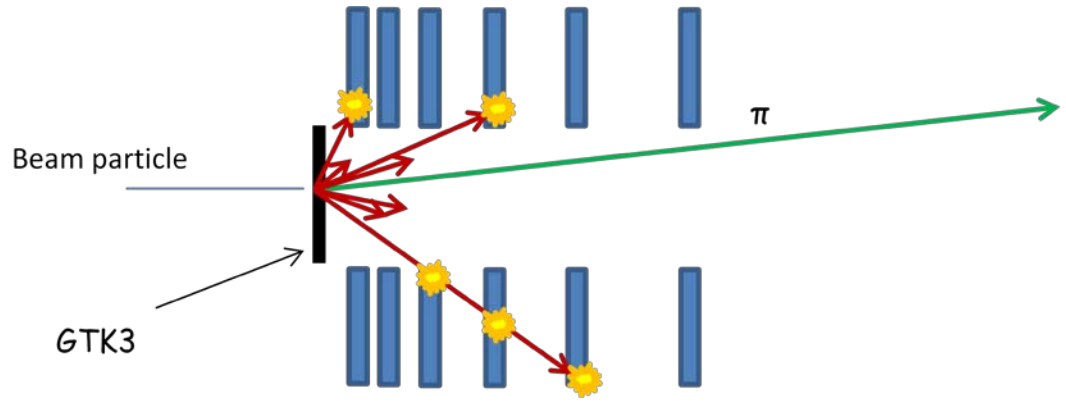

Figure 1 Despite the ulltra thin GTK detectors, beam particles can create accidental background if they undergo inelastic interaction in the GTK material. The scattered particles are revealed in the CHANTI which is placed immediately after the third GTK station.

Finally a veto for charged and neutral particles placed just downstream of the last GTK station, provides additional rejection of the accidental background coming from hadronic interactions of the beam particles in the last GTK station, as previously discussed. This detector, called CHANTI, consists of scintillators assembled in a rectangular shape surrounding the beam.

The CHANTI detector must be able to tag inelastic events with high efficiency. Given that it will be sensitive to the muon halo and to the inelastic interactions the expected rate of particles that release enough energy to be detected will be around 2 MHz. Even if it is not intended as a trigger veto at L0, the CHANTI must have a good time resolution (≤ 2 ns) to keep the random veto rate at an acceptable level: for instance, assuming a 5 sigma (10 ns) time coincidence window with the event fine time at reconstruction level, a 2% inefficiency on the signal would be induced by CHANTI

random vetoes. Although tracking capability may be not mandatory for the system, it can help in distinguishing beam halo events from inelastic interactions and in monitoring the beam halo itself very close to the beam. Last but not least, position sensitivity is useful in improving time resolution without increasing too much the granularity of the detector. Charge measurement is needed only to the extent of obtaining time slewing corrections, and, in the layout proposed, to improve the spatial resolution.

1.1.2 General Layout

The general layout of the system is sketched in Figure 2. It is composed of six stations, placed inside the vacuum tube respectively at 27-77-177-377-777-1577 mm distance from the GTK-3 (see Figure 2).

The rectangular hole inside each station is 50 mm in y and 90 mm in X due to the rectangular shape of the beam. Outer square side length is 300 mm. For particles hitting the GTK-3 center the CHANTI covers hermetically the angular region between 34 mrad and 1.38 rad wrt the beam axis, for particles hitting one of the GTK-3 corners the coverage is hermetic between 50 mrad and 1.16 rad. This must be compared to the highest angle under which a LAV station is possibly able to detect particles produced in the GTK-3 that is 49 mrad for particle produced at GTK-3 corner, so that LAV complements at low angles the information given by CHANTI. The CHANTI, by itself, is able to veto about 95% of all inelastic interactions of K in GTK-3 regardless of the final state. This vetoing efficiency reaches almost 99% if one restricts to potentially signal-like events, namely the ones where the kaon either did not survive the inelastic interaction or did not decay in the fiducial volume, and one track is reconstructed by the straw spectrometer.

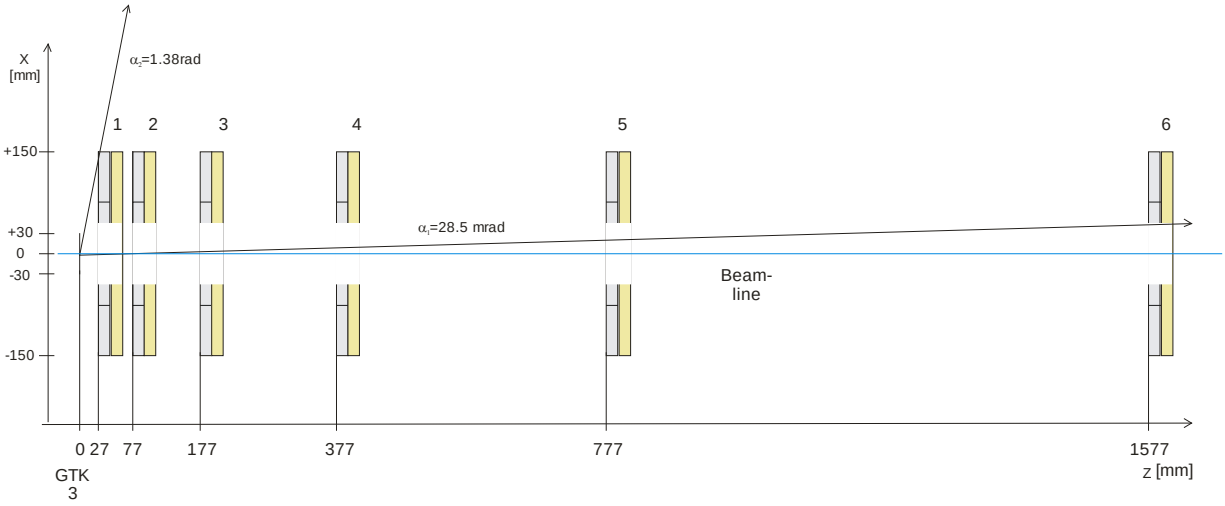

Figure 2 Positioning of the six CHANTI stations on the beam line (top view). The first colored line is GTK-3, the distance between GTK-3 and the first CHANTI station is 27 mm.

Each station is made up of two layers, called layer x and y respectively. A y(x) layer is composed of 22 (24) scintillator bars arranged parallel to the x(y) direction and individually shaped at the appropriate length (see Figure 3). Each layer is in the end composed by two sublayers, made up by 10+12

(10+14) bars, and staggered by half bar. Each bar is triangularly shaped, and two staggered bars face oppositely as shown in Figure 4.

Light is collected by means of one WLS fiber placed inside each bar and read at one side by a photodetector.

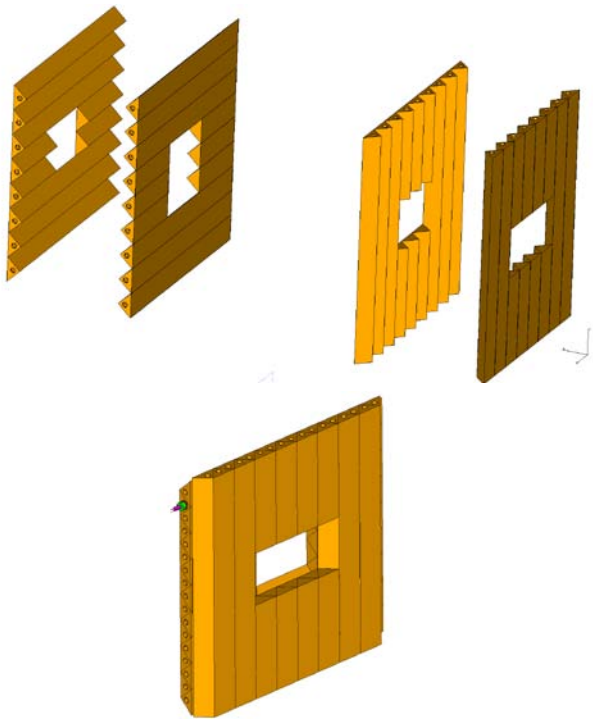

Figure 3 Layout of a complete CHANTI station. Top: exploded view; bottom: assembled station

1.1.3 Basic Scintillator Layout

Figure 4 Staggering of triangular scintillator bars to form a plane

The basic building block of the CHANTI is a scintillator bar in form of a triangular prism similar to the ones used in the D0 preshower detectors (1) and the MINERVA experiment (2) . It is produced at the NICADD-FNAL extruded scintillator facility (3) and consists of an extruded polystyrene core (Dow Styron 663 W) doped with blue-emitting fluorescent compounds (PPO 1% by weight and POPOP 0.03% by weight) and a co-extruded TiO_2 coating (0.25 mm thick) for reflectivity. The cross-section of the bar is a isosceles triangle with a base 33 mm and height of 17 mm, with a hole placed at 8.5 mm from the base . The hole has 1.7 mm diameter to host a WLS fiber. Optical glue ensures the coupling between the fiber and the scintillator. The main characteristics of the scintillator are:

- good LY (100% of Kuraray SCSN-81)
- radiation hardness (5% degradation observed after 1Mrad γ irradiation)
- Low cost
- fast response (τ few ns)

The WLS fiber used is Bicron BCF92 (4). The fiber is read only at one side, and in order to recover light emitted in the direction opposite to the photodetector it has been mirrored at one end, by means of Al sputtering in vacuum, using the same technique developed for the fibers of the ALICE EmC calorimeter (5). BCF92 has a very short fluorescence time (2.7 ns) and a light output and attenuation length comparable to the one of Kuraray Y11 .The WLS fiber is coupled to a SiPM device for photon detection.

The triangular shape allows a gap-free assembly when two bars are put one facing the other, in an almost self-sustaining shape. Moreover, the amount of light shared between two adjacent bars depends on the position of the impact point of the particle w.r.t. to the triangle centres (i.e. the position of the WLS fibers) This allows to determine the impact position in the direction orthogonal to the fiber with about 3mm resolution, much better than the one expected for rectangular shaped bars (roughly 10 mm) given the 33 mm spacing of the fibers .

1.1.4 Mechanics and Supports

The whole CHANTI detector consists of six stations which are placed inside a single vacuum tight vessel, together with the GTK-3 station. A possible solution using a rectangular vessel with a vacuum tight removable cover, is sketched in Figure 5 where the last GTK station and the CHANTI stations are visible. Mechanics and supports for GTK-3 will be the same as for the other two stations.

Each station is composed of scintillator bars glued together, so that they form a self-sustaining structure. A light Al frame is supporting mechanically each station to avoid any risk of ungluing and to fix the station to the outer vessel (see Figure 6).

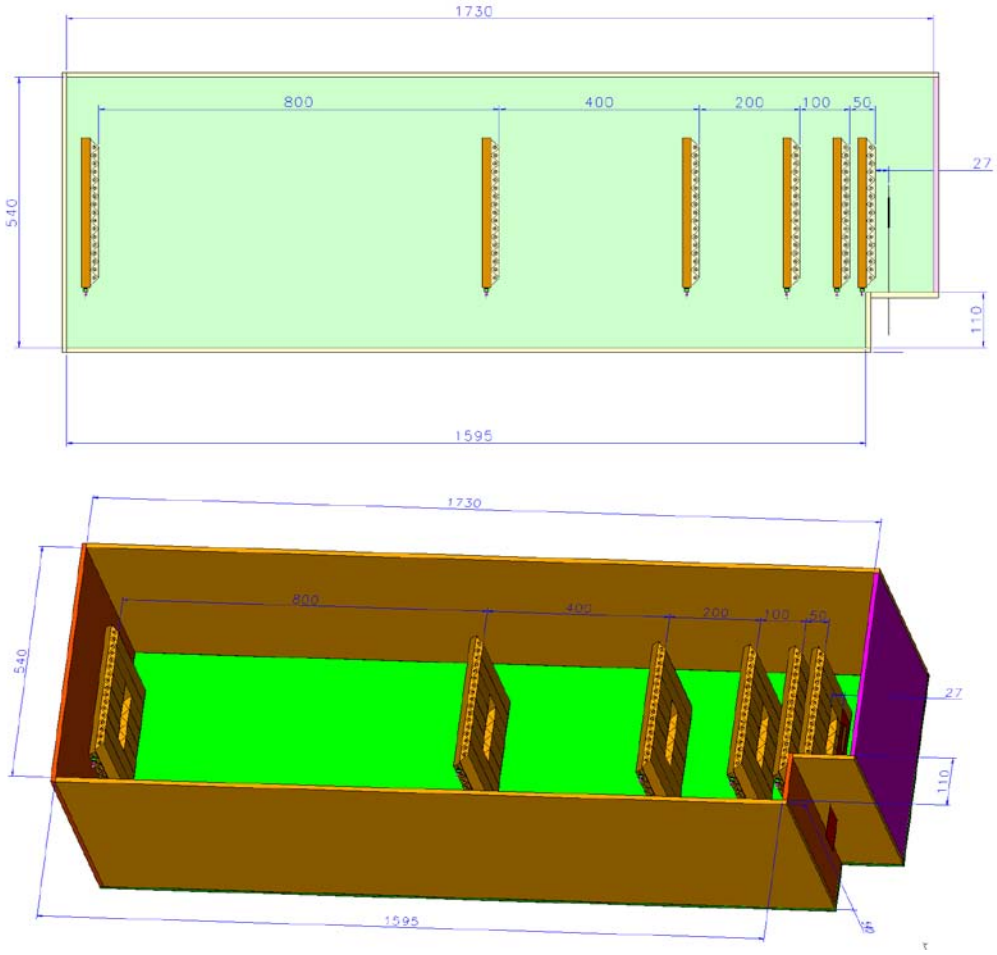

Figure 5 Layout for GTK-3 - CHANTI vessel. Vacuum flanges are not shown.

One station is composed of 46 bars with different length. The bars outside the beam gap are all of the same length, the so-called long bars (L). Since the gap is of rectangular shape, the bars in the central parts are of two different lengths, depending whether they are in the horizontal layer or in the vertical one. There are so-called middle (M) bars and short (S) bars respectively. The full lengths is 300mm (L), 117.5mm the middle type (M) and 102.5mm the short type (S). Table 1 summarizes the composition of one station.

Table 1 Lengths and number of long (L), middle (M) and short (S) type scintillators.

Bar type/Layer	*L*	*M*	*S*	**Total**
Layer Y	10	-	12	22
Layer X	10	14	-	24
Full station	20	14	12	46

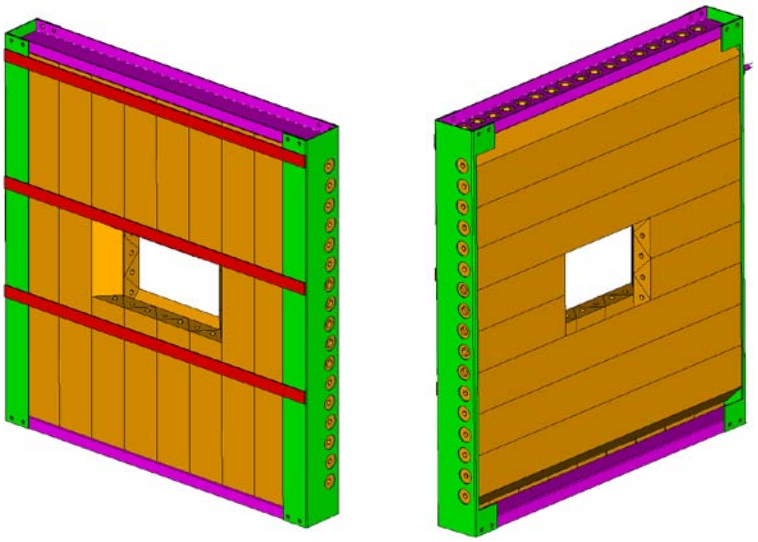

Figure 6 A sketch of a single CHANTI station, with the elements of the supporting frame (in green, violet and red). Left: beam view; right: rear view

Every scintillator bar is provided with a custom designed connector (see Figure 11) which is inserted in a precision hole (Ø 1.02 mm) and coupled to the photodetector. A precisely machined screw cap holds the photodetector in the right position. Alignment between the fiber center and the photodetector sensitive area is guaranteed at the level of 50 μm and is dominated by the tolerance in the position of the photodetector area w.r.t. its frame as provided by Hamamatsu.

It is worth to note that it is possible to substitute a photodetector by just unscrewing the connector. Moreover, quality tests can be easily arranged by using the same photodetector for all bars.

The precise definition of the position of the bars is given by a custom machined reference jig, (see Figure 16) on which each bar is placed "cusp down" to form a planar surface with the nominal dimensions. Bars in the orthogonal direction are then glued to these ones to form a "waffel – like" structure . The complementary bars are finally added in both directions to form the final planar station. See also 1.1.6, Figure 17 and Figure 18 for details.

Figure 18-e shows the final geometry with the readout connectors on the four sides of the station.

1.1.5 Photodetectors

The use of Silicon Photomultiplier (SiPM) devices as alternative to traditional photomultipliers tube (PMT) is becoming a widespread solution in particle detectors when high number of channels or high level of integration is needed.

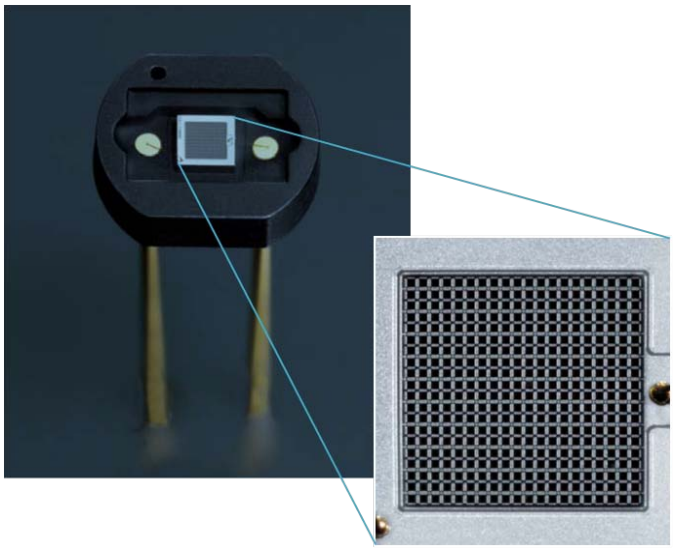

Figure 7 Hamatsu SiPM in ceramic packing

SiPM's are essentially (6) (7) (8) arrays of O(100) avalanche photodiodes (APD) (typical pixel size are 50x50 or 100x100 μm^2), see Figure 7, on one chip with shared readout in which each pixel is working in (quenched) Geiger mode (i.e. in a digital on/off configuration) but the number of firing pixels (and thus the overall response of the device) is proportional to the amount of incoming light (in the hypothesis Nphotons<<Npixels). Typical photon detection efficiencies (PDE) are highly dependent to SiPM model, they spread from 20-25% and can reach also 60-65% and gains are at level 10^5-10^6 (typical APDs gain are 10^2). This gain can be reached with no need for an HV system since the operation voltage is typically between 30 and 70 V and the leakage current of order of few nA. They can sustain very high rate, O(10 MHz) without problems. The dark rate (i.e. the rate observed with a counter at 0.5 pe threshold) , depending on manufacturer, on the pixel size and on the overvoltage, can vary from 100 kHz and few MHz at room temperature. It is not a concern if the number of expected photoelectrons is reasonably high, since it scales roughly by an order of magnitude per photoelectron as far as the threshold is increased to 1.5, 2.5, 3.5 pe and so on. Working with, for example, 3.5 pe threshold reveals a typical dark noise of about 100 Hz/channel.

SiPMs are intrinsically radiation hard devices. There is however, as for all semiconductor detectors, a known issue with their behaviour after intense neutron flux irradiations. The ASTM E722-93 standard practice allows to compare damage on silicon devices from different neutron sources by normalizing it to the damage induced by monoenergetic 1 MeV neutrons. In this context the figure of merit of an environment for SiPM devices is the number of equivalent 1 MeV neutron /cm^2 crossing the detector. It is known from literature (9) that a neutron irradiation corresponding to 4* 10^8 /cm^2 1 MeV equivalent neutron or less gives no visible effect on SiPMs, while increasing further the irradiation the dark noise starts increasing, reaching about 10 times its initial value at about 2-3 10^9 /cm^2 neutron fluence. Even if a 10 times larger noise w.r.t. to the standard one could still be manageable by increasing the threshold by 1-2 pe, we have checked that the radiation should be below this level at the CHANTI for at least two years of operation. Two different simulation have been carried out: the first, using FLUKA, has shown that the neutron dose at the CHANTI, generated by the primary proton beam on target should be of the order of 0.04 Gy/y which corresponds roughly to 10^8 n_{eq}/cm^2 /y. The second simulation has been done using GEANT4, to understand the

contribution to the neutron flux from the inelastic scattering of the beam in GTK, which were not considered in the first simulation. It has shown that the expected neutron fluence from GTK corresponds to less than 10^8 n_{eq}/cm^2 /y .Combining the two result we have that in two years running of NA62 the CHANTI SiPMs should integrate no more than 4 *10^8 n_{eq}/cm^2 i.e. should operate in safe conditions.

In order to choose the best solution for our photodetectors we tested some Hamamatsu SiPM series 13-50, 11-50 and 11-100 (first number 13 or 11 is the SiPM dimensions in tenths of millimeter, second number 50 or 100 is the pixel size expressed in microns). Hamamatsu provides, for each SiPM, specifications and working parameters as bias voltage, gain and dark rates, all of them measured at 25°C. In order to reproduce climatic conditions we used a thermostatic chamber that could fix temperature better than 0.1°C. A collimated Sr^{90} source has been used to compare different devices coupled to the same scintillator bar. Signals are amplified using a fast 10X amplifier. Data is collected using a Tektronix TDS5054 5GS/s oscilloscope via GPIB connection and a custom LabView program. Oscilloscope bandwidth is 500MHz, enough to follow few nanoseconds signal rise time.

Relative comparison in terms of number of photoelectrons collected is our figure of merit. First of all we measured for each SiPM single photoelectron response (SPR), this operation has been done using thermal-generated signals (dark noise) (see Figure 8). Once obtained the single photoelectron normalization factor the ratio signal/SPR for the irradiated bar could be used to compare different devices.

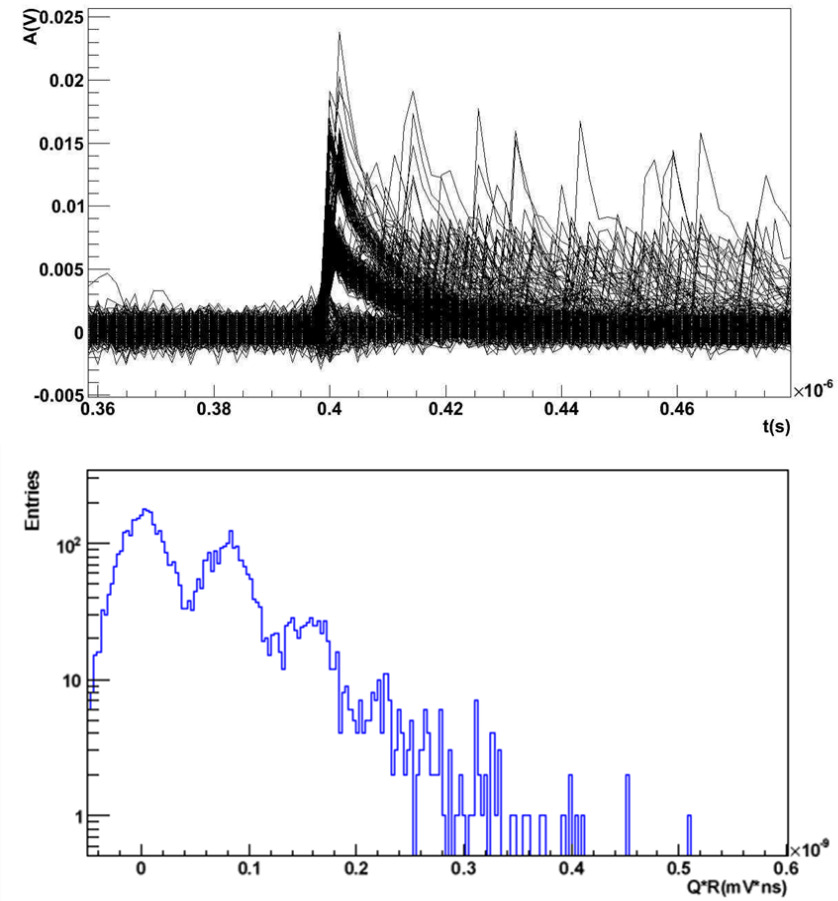

Figure 8 a) Thermal generated waveforms at 25°C. b) Dark noise spectrum obtained integrating waveforms shown on top.

Measured light yield for each SiPM is reported in Figure 9. We can conclude that SiPM serie 11-50 has a significantly lower photoelectron yield, while both 13-50 and 11-100 series seem viable solutions for our purposes.

In order to obtain an absolute scale of the expected number of photoelectrons (pe) the detector response was measured using cosmic rays. These tests show that for 300 mm long scintillator bars, equipped with (mirrored at one side) BCF92 fibres and Hamamatsu SiPMs (Type: S10362-13-050-c Ø=1.3 mm, with 50 X 50 μm^2 pixels) more than 100 pe are generated per detector plane, if crossed by straight MIPs i.e. more than 50 pe per channel/ MIP.

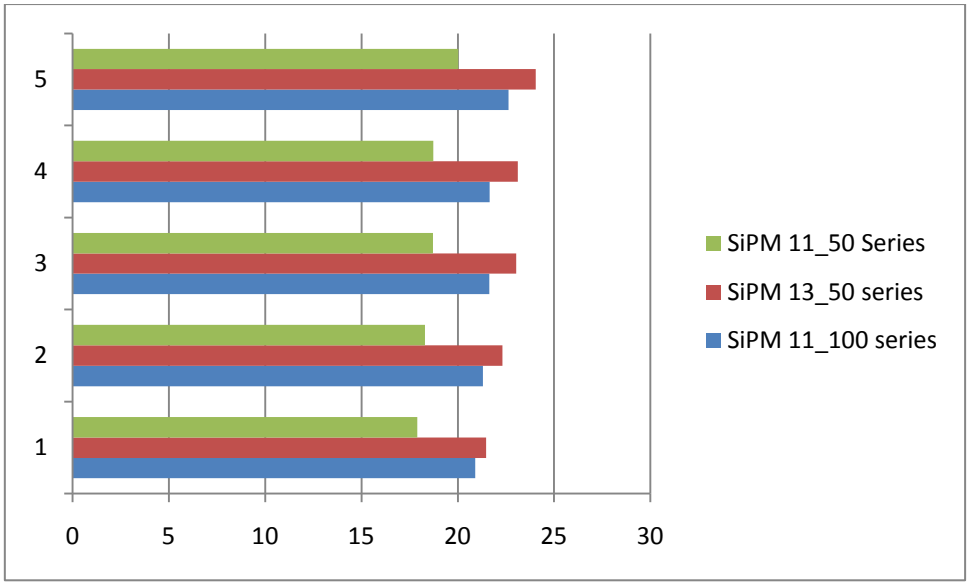

Figure 9 Photoelectron yield for photodetectors of three different Hamamatsu SiPM series. Five photodetectors have been measured for each series using the Sr^{90} source.

This allows to operate the device with a threshold in the range of 3-4 pe per channel or more with negligible efficiency losses.

Time resolution using the fast fluorescent Bicron BCF92 fiber has been measured (see Figure 10) to be about 800 ps for MIPS crossing the detector at a fixed distance from the SiPM: for an event with full x-y reconstruction this is thus the expected time resolution, well in line with the CHANTI specifications.

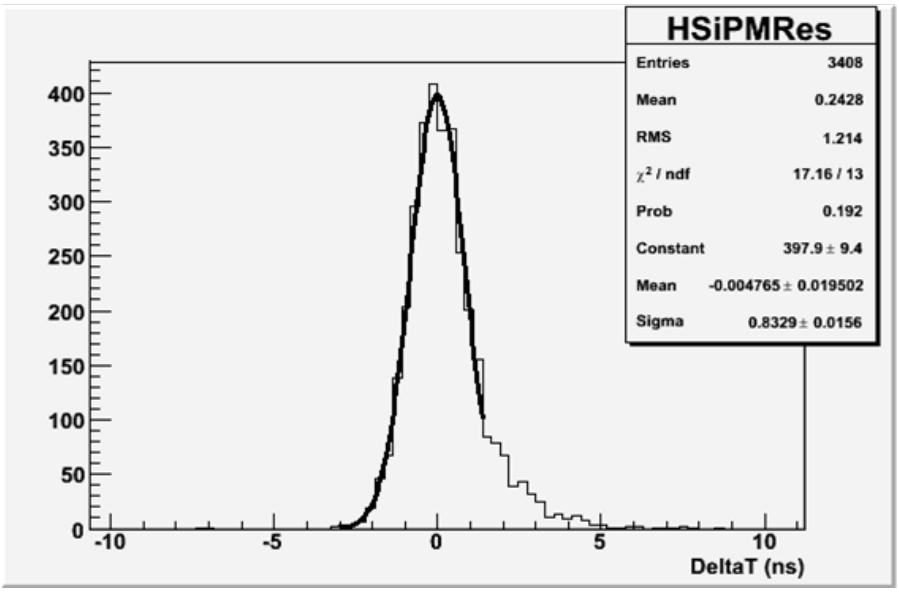

Figure 10 Time resolution measured for a triangular bar equipped with a Bicron BCF-92 fiber readout using a FBK-IRST SiPM.

1.1.6 Prototype construction

CHANTI prototype has been assembled in Napoli at the end of July 2010. It is a full dimension prototype of a X-Y station. Scintillator bars for the prototype were obtained courtesy of FNAL and Al sputtering of the fibers was performed at LNF.

The construction procedure adopted is hereby briefly described.

First, some custom tools to simplify the mechanical assembly were developed.

The assembly took about 20 days, and can be divided in three main parts:

1) Gluing fibers into bars,

2) Test of the bars,

3) Assembly all test-passed bars into final X-Y station.

A single X-Y station contains three different types of bars: 300mm (L), 117.5mm (M) and 102.5mm (S).

All operations have been done in a class 100 clean room environment and all components have been accurately washed using an ultrasound cleaning before manipulation.

1.1.6.1 Gluing of the Fibers into the Scintillator Bars.

This operation is itself done in two steps. First mirrored fibers and connectors are glued together and finally this ensemble is glued into a bar.

1.1.6.1.1 Fibers-Connectors Gluing

Each connector is provided together with a Teflon© cap. It is a multi-purpose tool (Figure 11) to define a reference plane for the fibers as well as to protect the polished side of the fiber during transport and handling.

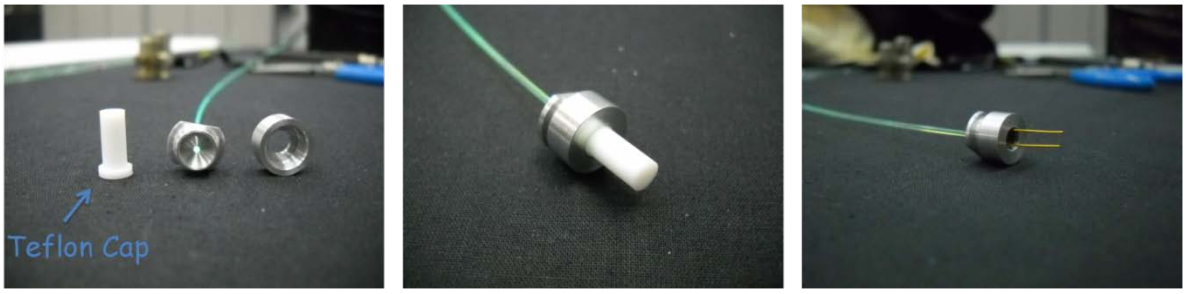

Figure 11 a) Connector in its parts b) Assembled connector c) Connector with SiPM

During the prototyping phase different glues were tested and the epoxy ARALDITE 2011 was found the best choice for this application. It has a high viscosity which helps to prevent glue leaking into the wrong connector side. This glue is also solvent-free avoiding cladding damages. Optical properties are not important at this level, because no coupling is required.

Fibers are plugged in their final position into connector, being careful they reach the Teflon cap. A special support (Figure 12) has been developed in order to parallelize this operation. It is able to carry 24 fiber-connector couples. When the fiber is in its correct position glue is put using a syringe (with a Ø 1.3mm needle).

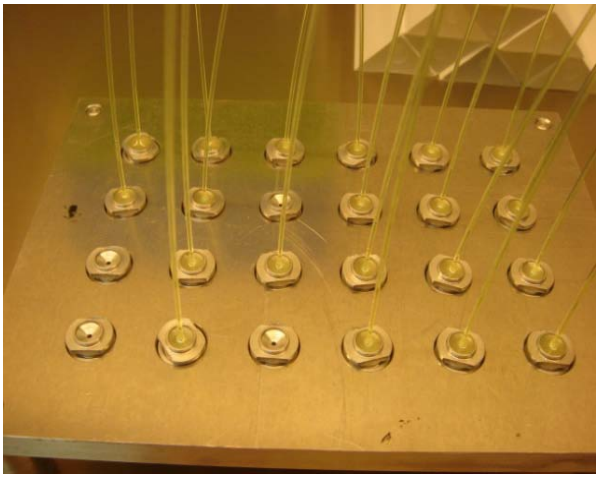

Figure 12 Tool for connector-fiber gluing.

Figure 13 The fiber-bar gluing tool in action.
Its back side is identical to the one shown.
Glue is injected from bottom using syringer.

1.1.6.1.2 Fibers-Bar Gluing.

Once obtained the fiber-connector ensemble they were glued into the bars. A custom tool (Figure 13) allowing to fix the bars in vertical position was developed. It can host up to 10 bars, and was used to hold the bars during the hardening of the glue. Five days are necessary to glue all the bars for one station.

Glue used is a SCIONIX Silicon Rubber Compound, that guarantees a good fiber-scintillator optical coupling and is known from NASA database (10) to be low outgassing.

The glue is injected from the bottom using again a syringe, this method was found to reduce the risk of trapping air bubbles in the glue. The required glue quantities are adapted for each bar length (L -> 2.1ml, M -> 1.0ml, S -> 0.9ml). This is important in order to avoid leaking at the top of the bar. The whole prototype contains about 65ml of glue.

1.1.6.2 Scintillator Bar Test.

Since after complete assembly any bar substitution is impossible a quality test before assembly is needed. For each bar the response to a Sr^{90} collimated beta-source is measured. Measurements have been carried out with the same setup described in section 1.1.5 for the SiPM comparison, in a controlled temperature environment using the same photodetector (an Hamamatsu 13-50 type) coupled each time to a different bar. Experimental apparatus is in Figure 14.

Figure 14 Experimental apparatus for bar test. a) Setup overview on the right the readout electronics and amplifier. b) Collimator detail. c) Source in finial position.

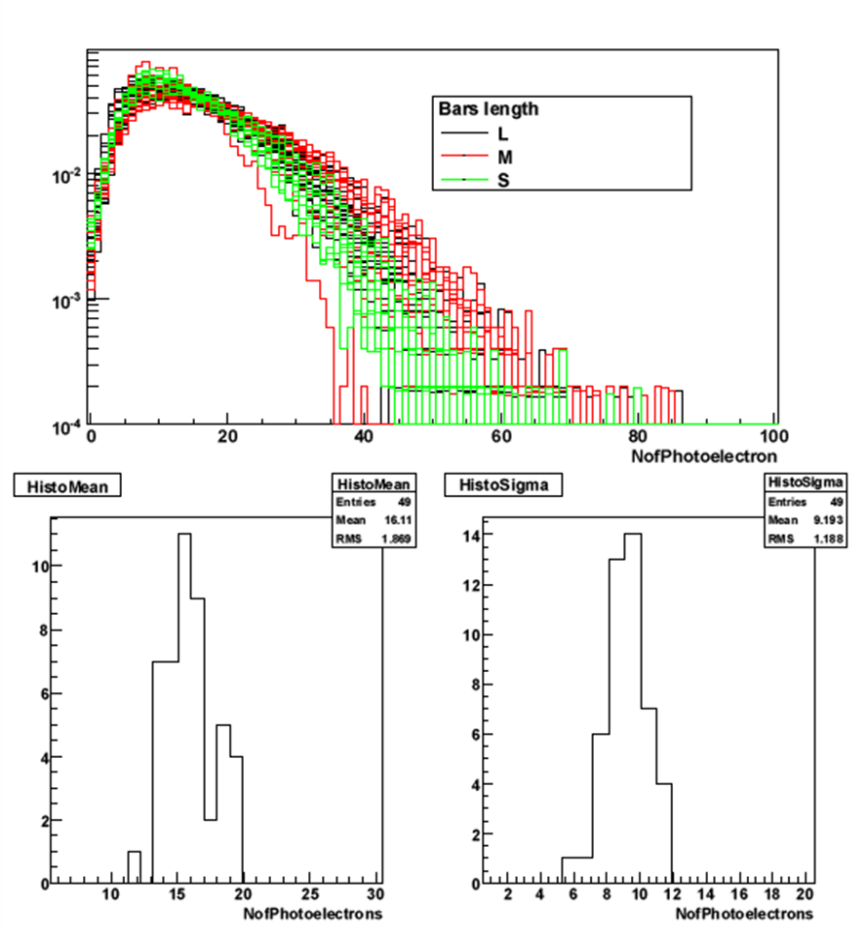

Figure 15 Bars quality test: a) Measured Spectrum for the different scintillators, b) Measured spectrum mean value, c) Measured spectrum RMS

Relative comparison among different bars in terms of number of photoelectrons collected is again our figure of merit.

Figure 15a shows all bars normalized source-response in terms of number of photoelectrons. Mean values for each curve are given in Figure 15b : one can conclude that the bars quality is very uniform. Only one bar showed a significant difference, the cause of low light response was understood, after inspection of the bar: the fiber edge was found slightly backward with respect to its reference plane facing the SiPM sensitive surface, leading to lower light collection efficiency.

1.1.6.3 Module Assembly

Once all the material was ready, a prototype could be assembled in 2 steps. Each step takes one day.

During the first day a half-layer X and Y are glued together. First of all bars are arrange on a jig (Figure 16), afterwards glue points are defined using a Teflon mask (Figure 17). Then the bars of the other half-layer were aligned on top. A second jig is put on top of the assembly to align the last half-layer. Pressure is added to increase the glue uniformity. Each glue spot contains 0.1ml of glue.

Figure 16 Jig used to align bars during gluing, on top Teflon mask to distribute glue spot

On the second assembly day the prototype is completed. Figure 18 shows all the steps of the procedure. First of all bars of a half-layer are aligned on the jig and glue spots are applied (3 for L-type bars and 2 for M and S type bars). Then the complementary half-layer is put on top. Again glue spots are placed and the last half-layer placed. A weight has been applied in order to uniformly distribute glue. For the whole module about 9.5 ml of structural low outgassing epoxy glue (3M DP490), identical to the one used for the reinforcement of the LAV blocks, were used. .

Figure 17 Assembling "First step": a) A half-layers is arranged on the jig, b)Teflon mask is aligned, c) Glue spots are applied, d) Mask is removed, e) f) Bars of the other half-layer are placed, g) h) second jig is applied on top to align last placed half-layer and to redistribute pressure, i) Half-module as appear the day after gluing

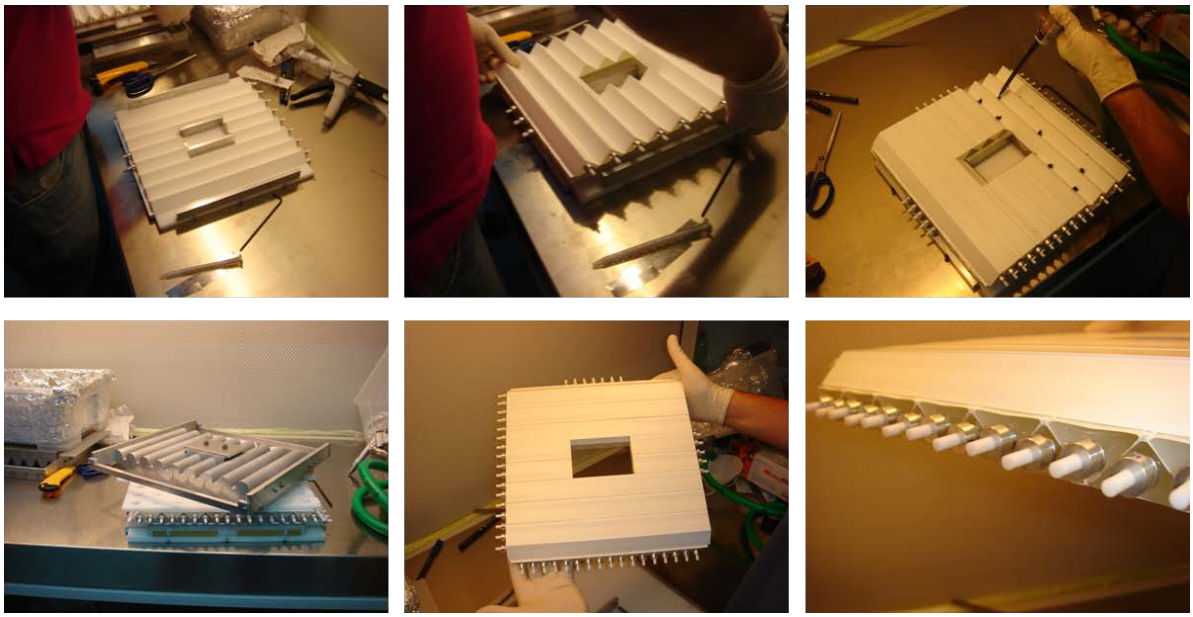

Figure 18 Assembling "Second step": a) Half-layer bars ready to be glued to half-module, b) Gluing half-module, c)Last half-layer gluing, d) Weight applied, e) Prototype as appears after one day, f) Connectors detail

1.1.7 Readout

The conceptual scheme of the CHANTI readout is shown in Figure 19.

As previously sketched each scintillator bar is coupled individually to a SiPM which converts light collected by the fiber into electrical signals. Each SIPM has two pins which are used both to polarize it and to read these signals.

The bias voltage is brought to the SiPMs inside and the signal are carried out from the vacuum tube using appropriate vacuum tight flanges as done for the LAV signals and HV. Both twisted pair and coaxial cables are being investigated as possible solution for the internal cabling , the final choice being the one which optimizes cost/benefits ratio.

A small amplification board is placed just outside vacuum in order to be able to transfer signals from the detector to the FEE crate with an acceptable S/N level.

Typical signals are expected of order few mV (on 50 Ω impedance) with a fast rise time (1 ns) and a somewhat long decay time (in the range 10-100 ns). The maximum expected rate in input to the FEE will be, for the inner bars, of the order of about 1 MHz per bar, as shown by Geant4 simulations, plus the dark rate (for Hamamatsu SiPMs, some 100 kHz). In order to keep some safety factor, the electronics will be designed to cope with a 5 MHz rate.

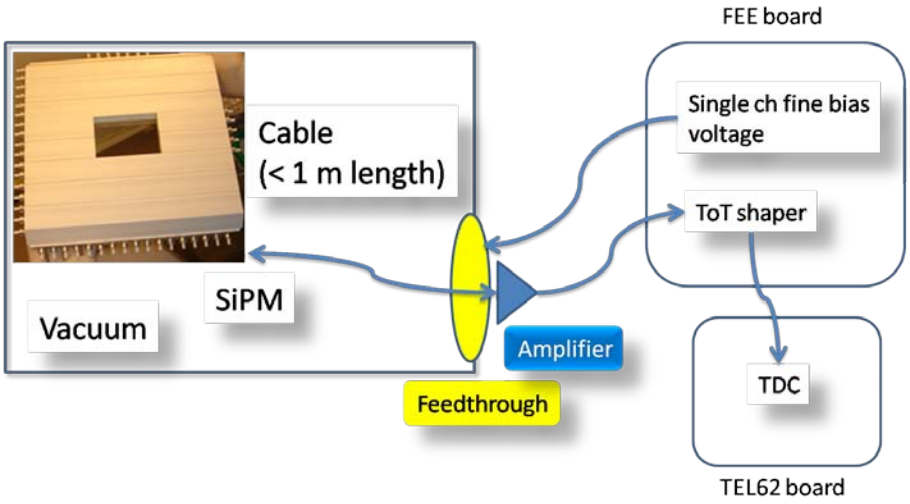

Figure 19 Conceptual scheme of the CHANTI readout.

1.1.7.1 FEE

The FEE boards provide for each channel:

- a way to control the V_{bias} with O(10 mV) accuracy
- a fast, DC coupled, conversion to a Time Over Threshold-LVDS signal output
- a temperature and/or a dark current (with nA resolution) monitor for slow control adjustment of the V_{bias}

Thresholds and V_{bias} settings will be controlled using the CANOpen standard.

The LVDS output will be directly sent to a TEL62 board equipped with HPTDC for both leading and trailing edge measurement. The total number of channels needed is 46 X 6 = 276. One TEL62 board equipped with three 128 ch TDC boards will be able to readout the whole system and provide also a large number of spare channels.

The TOT technique will allow also approximate charge measurement to improve the spatial resolution of the system.

1.1.7.2 Integration with Trigger/DAQ

The CHANTI is not supposed to give primitives for the L0 trigger. It uses the standard TEL62/HPTDC structure and obtains the clock via the LTU+TTCex system.

An evaluation of the maximum data rate can be done as follows. The highest multiplicity in the CHANTI is expected from the beam halo events, who cross all six stations. If fully efficient on these events the system will give at most 4 X 6 = 24 hits or 192 bytes per event. These events occur at 1 MHz rate. Inelastic interactions in the GTK will be detected at approximately the same rate, with comparable hit multiplicity. One can safely estimate a maximum of 200 bytes at 2 MHz. Assuming a 1 MHz trigger rate and a readout time window of O(100 ns) one expects O(200 kHZ) of such events in coincidence with a trigger. This would generate a data rate of about 40 MB/s well below the TEL62 specifications.

1.1.7.3 External Services

The external services needed for the CHANTI are power for the crate and for the common Vbias generator, and the CANOpen system for the DCS.

Bibliography

1. **D0 Collaboration.** The upgraded D0 Detector. *Nucl. Instrum. Methods A565,413.* 2006.

2. **MINERVA Collaboration.** The Physics Case and Technology of the MINERvA Experiment. *MINERvA Document 218-v4.* 2006.

3. **Beznosko, D. et al.** Nuclear Science Symposium Conference Record - IEEE, 790-793, vol.2. 2004.

4. Saint-Gobain. *http://www.detectors.saint-gobain.com.* [Online]

5. **F. Ronchetti (on behalf of the ALICE Collaboration).** *Journal of Physics: Conference Series 160 012012.* 2009.

6. **Buzhan, P. et al.** *Nucl. Instrum. Methods A504, 48.* 2003.

7. **Sadygov, Z. et al.** *Nucl. Instrum. Methods A504, 301.* 2003.

8. **Golovin, V. and Saveliev, V.** *Nucl. Instrum. Methods A518, 560.* 2004.

9. *Silicon Photo-Multiplier radiation hardness tests with a beam controlled neutron source.* **Angelone, M. et al.** Submitted to Nucl. Inst. Meth. A. arXiv: 1002.3480.

10. NASA. *http://outgassing.nasa.gov/.* [Online]

NA62 Acronyms and Abbreviations

ADC	Analog to Digital Converter
AM	Absorber Module
APD	Avalanche PhotoDiode
ASIC	Application Specifc Integrated Circuit
BCRST	Bunch Counter ReSeT
BEATCH	Progran to provide coordinates of all beam elements as input for alignment
BEND	BENDing magnet or dipole
BIF	Barrier Improvement Factor
CALB	Sub-detector data format for calibration
CCPC	Credit-Card PC: commercial processor on TELL1/TEL62 boards
CEDAR	Cerenkov Differential counter with Achromatic Ring Focus: differential Cerenkov detector developed at CERN
CHANTI	Charged ANTI
CHOD	Charged HODoscope
CKM	Cabibbo–Kobayashi–Maskawa matrix
CM	Circulation Module
COLL	COLLimator
COND	Condition data of the detector (extracted from DCS)
CONF	configurations of the run, including active detectors, trigger configurations, beam conditions, etc.
COST	calibration parameters computed by calibration tasks running on (partially or fully) reconstructed data.
COTS	Commercial-Of-The-Shelf
CPD	Calorimeter Pipeline Digitizer module
CREAM	Calorimeter Readout Module
CTL	Chamber Trigger Logic for straws L0 trigger system
DAQ	Data Acquisition System
DCS	Detector Control System
DDR2	Double Data Rate SDRAM (memory chips)
DIM	Distributed Information Management system
DLL	Delay Locked Loop
DLS	Data Logging System
DM	Distribution Module
DPRAM	Dual Ported RAM
DRAM	Dynamic RAM
EB	Event-Building
ECN3	Experimental Cavern housing the NA62 experiment
ECRST	Event Counter ReSeT
EDX	Energy-Dispersive X-ray spectroscopy
EE	End of Ejection
EOB	End Of Burst
EOC	End Of Column option for GTK chip architecture

EoC	End-of-Column part in the P-TDC chip architecture of the GTK
EOF	End Of Frame
FADC	Flash Analog to Digital Converter
FE	Front-End
FEE	Front-End Electronics
FEM	Finite Element Model
FIFO	First In First Out buffer
FISC	Filament Scanner, a beam profile detector inside the beam vacuum system
FNAL-NICADD	Fermi Nat Lab - Photo injector Lab (18Mev electron linac)
FPGA	Field Programmable Gate Array
FR	Fast Reconstruction
GbE	Gigabit Ethernet
GIM	Glashow–Iliopoulos–Maiani mechanism which suppresses flavour-changing neutral currents)
GOL	Gigabit Optical Link transmitter
GPN	General Purpose Network
GPU	Graphic Processing Unit
GTK	GigaTracker
HALO	A beam simulation program to calculate muon HALO rates
HPTDC	High Performance Time to Digital Converter
HV	High Voltage
IRC	Intermediate Ring Calorimeter
JTAG	Joint Test Action Group protocol
L0	Level 0 Trigger
L0TP	Level 0 Trigger Processor
L1	Level 1 trigger
L1TP	Level 1 Trigger Processor
L2	Level 2 trigger
LAV	Large Angle Veto
LED	Light-Emitting Diode
LG	Lead Glass
LGTS	Lead Glass Test Station
LKr	Liquid Kripton calorimeter
LTU	Local Trigger Unit
LV	Low-Voltage
LVDS	Low-Voltage Differential Signalling
MBPL-TP	Dipole Bending Magnet with Tapered Pole
MEPs	Multi-Event Packets
MIP	Minimum ionising particle
MNP33	NA62 Experimental Magnet
MUV	Muon Veto System
NAHIF	North Area High Intensity Facility
NIM	Nuclear Instrumentation Module
NINO	Fast front-end preamplifier-discriminator chip developed by ALICE
NNLO	Next-to-next -to-leading order
PCB	Printed Circuit Board

PDE	Photon Detection Eff.
Pe	Photo-electron
PECL	Positive Emitter-Coupled Logic
PEI	PolyEtherImide
PET	PolyEthylene Terephthalate
PMT or PM	Photomultiplier Tube
POPOP	1,4-bis(5-phenyloxazol-2-yl) benzene organic scintillator
PP-FPGA	Pre-Processing FPGA in the TELL1/TEL62 boards
PPO	2,5-Diphenyloxazole organic scintillator
PTP	Para-TerPhenyl
PVSS	Object-oriented process visualization and control system by ETM (a commercial SCADA system)
QCD	Quanten Chromodynamik
QDR-II	Quad Data Rate II memory
QPLL	Quartz-crystal based Phase-Lock Loop
QUAD	QUADrupole
RECO	Data format for fully reconstructed events
RICH	Ring Imaging Cherenkov
SAC	Small Angle Calorimeter
SAV	Small Angle Veto
SDRAM	Synchronous Dynamic Random Access Memory
SEM	Scanning Electron Microscope
SiPM	Silicon PhotoMultiplier
SOB	Start of Burst
SL-FPGA	Sync-Link FPGA in the TELL1/TEL62 boards
SLM	Smart Link Modules
SM	Standard Model of particle physics
SPI	Serial Port Interface
SPR	Single Photoelectron Response
SRAM	Static Random Access Memory
SRB	Straw Readout Board
TCC8	Target Chamber Cavern upstream of ECN3
TDAQ	Trigger and Data Acquisition system
TDC	Time to Digital Converter
TDCB	Time to Digital Converter Board
TDCC-FPGA	TDC Controller FPGA in the TDC boards
TEL62	Trigger and Data Acquisition board developed for NA62, based on TELL1 design
TELL1	Trigger ELectronics for L1 trigger: readout board developed by LHCb
THIN	Data format for summary data from fully reconstructed events
TRIM	Steering Magnets for the Beam
TTC	Timing, Trigger and Control
TTCex	TTC encoder VME board developed by CERN
TTCrq	TTC receiver mezzanine card developed by CERN
TTCrx	TTC receiver ASIC developed by CERN
TURTLE	Trace Unlimited Rays Through Lumped Elements, a beam tracking and simulation program

VME	Electronic bus and rack standard
VTL	View Trigger Logic for straws L0 trigger system
WE	Warning of Ejection
WLS	Wave-Length Shifting
WWE	Warning of Warning of Ejection